Appl. Phys. B 58, 295–301 (1994)

Applied Physics B Lasers and Optics

A New Ring Trap for Frequency-Standard Applications

M. Kajita, A. V. Zvyagin*

Kansai Advanced Research Center (K.A.R.C.), Communications Research Laboratory, Ministry of Posts and Telecommunications, 588-2 Iwaoka, Iwaoka-cho, Nishi-ku, Kobe 651-24, Japan (Tel.: +81-78/969-2151, Fax: +81-78/969-2144)

Received 22 June 1993/Accepted 13 December 1993

Abstract. We propose a new ring ion-trapping system, that is advantageous for use in frequency-standard applications and ultrahigh-resolution spectroscopy. The ring trap can store a large number of ions with low susceptibility to the second-order Doppler effect. The ring-trap electrodes also form a wide-band microwave cavity. Microwave radiation trapping during the probe cycle makes it possible to meet the Lamb-Dicke criterion more satisfactorily than with an rf/dc hybrid linear trap, in which traveling microwave power is used. This technique yields an increased S/N ratio because the microwave probing power is absorbed in the fundamental mode rather than in the sidebands induced by ion motion in the trap. This paper presents an analytical model of the ring-trap system and estimates of the main parameters of the ring trap.

PACS: 06.00, 07.60

Techniques for confining charged particles in a restricted space have many applications, particularly in ultrahigh-resolution spectroscopy. Of great practical interest is the application of the ion-confining technique to frequency standards [1]. The superior performance of ion frequency standards is due to the isolation of the ions from other objects, which eliminates the frequency shift due to wall collisions. Furthermore, one can observe the spectrum with a narrow linewidth, because the interaction time between ions and the probe field can be long. The highest Q values of hyperfine transitions (4×10^{11} for $^{171}Yb^+$ [2] and 1×10^{12} for $^{199}Hg^+$ [3]) have been obtained using the ion-trap technique. However, the second-order Doppler effect is the main limiting factor for the accuracy of atomic clocks based on ion traps, especially if a radio-frequency (rf) trap is used to store the ions. This effect is due to rf heating whose magnitude increases as the density of the ions in the trap increases. A reduction of the rf-heating effect can be obtained by lowering the number of trapped ions, but this leads to a lower Signal-to-Noise (S/N) ratio of the spectrum.

Recently, Prestage et al. developed a hybrid rf/dc linear trapping system that can confine 20 times as many ions as an ordinary 3-dimensional Paul trap with the same second-order Doppler effect [3–5]. Use of this trapping technique in the $^{199}Hg^+$ frequency standard reduced the instability to less than 2×10^{-15} averaged over 24000 s [3].

We propose a new ring-type ion-trapping system that consists of two coaxial cylindrical electrodes enclosed by two flat lid electrodes. Ions of the required e/m ratio can be stably trapped if a specific combination of ac and dc voltages is applied to the ring trap electrodes. The ring trap electrodes also form a microwave cavity. We show that it is possible to increase the S/N ratio by producing an appropriate microwave mode in the ring-trap cavity. The combination of ion trapping and microwave properties of the ring-trap model permits ultrahigh-resolution spectroscopic investigations in the microwave region because of a highly developed optical microwave double-resonance technique [1–6].

The ring trap (consisting of 4 bar electrodes) was originally proposed for the investigation of light atomic ions using an $L - C$ tuned circuit [7]. Presently, this ring-trapping system is being used for ion cooling and crystallization experiments [8]. Simultaneous trapping of both ions and microwaves in the conventional Paul trap has also been investigated [9]. In this paper, we present the first proposal to trap both microwave radiation and ions in the ring trap and apply it to a frequency standard. As an example, we present an analytical model of the ring trap, trapping $^{199}Hg^+$ ions and observing the hyperfine transition at 40.6 GHz. The $^{199}Hg^+$ ion seems to be the most promising for frequency-standard applications because of its

—large atomic mass, which leads to a smaller second-order Doppler effect;

* S.T.A. fellow invited to K.A.R.C. Permanent address: Institute of Metrology for Time and Space (VNIIFTRI) Mendeleevo, 141570 Moscow, Russian (Tel: +7-095/535-9337, Fax: +7-095/535-7386)

—large hyperfine transition frequency, which allows use of a higher Q factor for the clock transition; and
—low sensitivity to magnetic field variations.

1 Trapping Property of the Ring Trap

The ring trap electrode configuration can be obtained geometrically by rotating Fig. 1 around the z-axis of the cylindrical coordinate system. The electrodes thus consist of two coaxial cylinders with radii R_1 and R_2 ($R_1 < R_2$), and upper and lower lids. Adjacent electrodes must be electrically isolated. Applying the voltages

$$V = \begin{cases} V_{ac1} + V_{dc} & \text{cylinder } r = R_1\,, \\ V_{ac2} & \text{cylinder } r = R_2\,, \\ \text{Ground} & \text{upper and lower lids}\,, \\ V_{aci} = V_{0i}\cos\Omega\,, & i = 1,2 \end{cases} \tag{1}$$

provides a force that causes a charged particle to vibrate around a point where this field is the weakest. The trapping conditions thus obtained can be described in terms of a pseudopotential well [10]. To analyze the conditions required for stable trapping of the ion, we calculated the trapping potential analytically, ignoring the space-charge effect. This analysis is also important to find a condition to localize ions at a convenient place when the ring trap is applied for the frequency standard.

The potential inside the ring trap consists of

—the pseudopotential Ψ created by a time-varying inhomogeneous electric field (V_{ac}), and the
—potential Φ_{in}, generated by applying a dc bias to the inner-cylinder electrode (V_{dc}). The potential Φ_{in} is intended to improve the pseudopotential in the trap. The Ψ and Φ_{in} values are calculated separately and then summed.

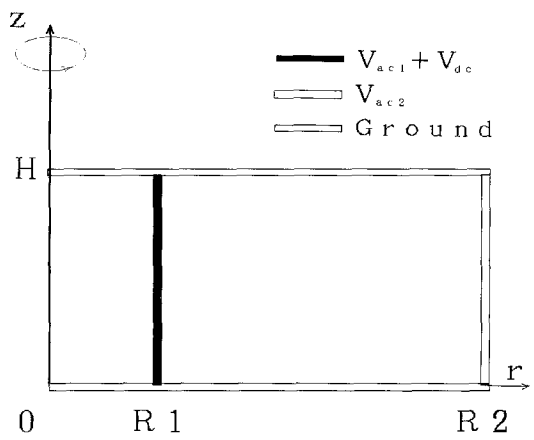

Fig. 1. Geometry of the analytical model of the trapping system. The rectangle in the r–z-plane should be rotated around the z-axis to obtain two coaxial cylinder electrodes enclosed by two lids. Adjacent electrodes are electrically isolated

1.1 Calculation of the Pseudopotential

An expression for the pseudopotential can be derived from the electric field expression in the trap at a given moment in time. Using the method of separation of variables to solve the Laplace equation in cylindrical coordinates, an

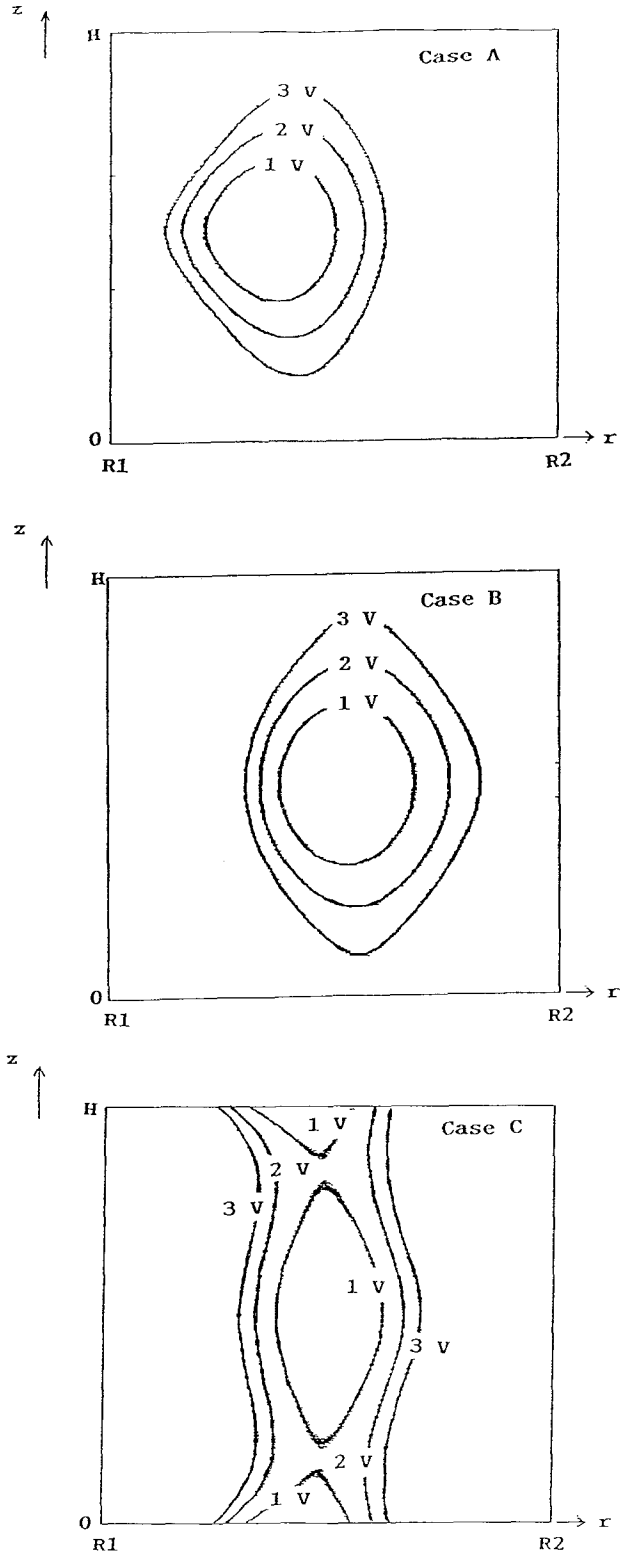

Fig. 2. Contour plot of the ring-trap pseudopotential. Trapping conditions are listed in Table 1

analytic expression for the electrostatic potential Φ is obtained. Noting the rotational symmetry of the electrodes considered here, the potential does not depend on the angular cylindrical coordinate θ, and so the general solution can be written as

$$\Phi(r,z) = \sum_{k=0}^{\infty} [A_k I_0(\pi k r/H) + B_k K_0(\pi k r/H)] \sin(\pi k z/H) , \tag{2}$$

where I_0 and K_0 are zero-order modified Bessel functions, and A_k and B_k are constants determined by boundary conditions. For the geometry shown in Fig. 1 and the applied voltage given in (1) (with $V_{dc} = 0$), the boundary conditions are

$$\Phi(r,z) = \begin{cases} V_{ac1}, r = R_1, 0 < z < H , \\ V_{ac2}, r = R_2, 0 < z < H , \\ 0, z = 0, R_1 < r < R_2 , \\ 0, z = H, R_1 < r < R_2 . \end{cases} \tag{3}$$

The electrostatic potential can be written as

$$\Phi(r,z) = \frac{4V_{ac1}}{\pi} \sum_{k=\text{odd}} \frac{1}{k} \times \frac{(\gamma K_0^{(1)} - K_0^{(2)}) I_0\left(\frac{\pi k}{H} r\right) + (I_0^{(2)} - \gamma I_0^{(1)}) K_0\left(\frac{\pi k}{H} r\right)}{K_0^{(1)} I_0^{(2)} - K_0^{(2)} I_0^{(1)}} \times \sin\left(\frac{\pi k z}{H}\right), \tag{4}$$

where $\gamma = V_{02}/V_{01}$, $K_0^{(i)} = K_0(\pi k R_i/H)$, and $I_0^{(i)} = I_0(\pi k R_i/H)$, $i = 1, 2$. According to the theory developed by Dehmelt [10], one can obtain the trapping pseudopotential by averaging the time-varying inhomogeneous field in the trap over one period of oscillation:

$$\Psi = (e/4m\Omega^2)\,(\text{grad}\,\Phi)^2 , \tag{5}$$

where e is the elementary charge and m is the ion mass. The gradient of the electrostatic potential can be written in terms of the electric field components as

$$[\text{grad}\,\Phi(r,z)]^2 = E_r^2 + E_z^2 . \tag{6}$$

Finally, the pseudopotential inside the ring trap is expressed as

$$\Psi(r,z) = (e/4m\Omega^2)(E_r^2 + E_z^2) , \tag{7}$$

where

$$E_r(r,z) = -\frac{4V_{01}}{H} \sum_{k=\text{odd}} \times \frac{(\gamma K_0^{(1)} - K_0^{(2)}) I_1\left(\frac{\pi k}{H} r\right) - (I_0^{(2)} - \gamma I_0^{(1)}) K_1\left(\frac{\pi k}{H} r\right)}{K_0^{(1)} I_0^{(2)} - K_0^{(2)} I_0^{(1)}} \times \sin\left(\frac{\pi k z}{H}\right), \tag{8}$$

$$E_z(r,z) = -\frac{4V_{01}}{H} \sum_{k=\text{odd}} \times \frac{(\gamma K_0^{(1)} - K_0^{(2)}) I_0\left(\frac{\pi k}{H} r\right) + (I_0^{(2)} - \gamma I_0^{(1)}) K_0\left(\frac{\pi k}{H} r\right)}{K_0^{(1)} I_0^{(2)} - K_0^{(2)} I_0^{(1)}} \times \cos\left(\frac{\pi K z}{H}\right), \tag{9}$$

and $I^{(1)}$ and $K^{(1)}$ are first-order modified Bessel functions.

Figure 2 shows equi-pseudopotential lines inside the ring trap obtained by numerical calculation using the trapping parameters listed in Table 1. Figure 3 presents the dependence of the pseudopotential on the r-coordinate when z is fixed ($z = H/2$). It is clear that if V_{01} and V_{02} are equal (Case A), the pseudopotential minimum is not midway between the coaxial electrodes, but is shifted toward the inner electrode. The value of r for which the pseudopotential is minimum $r = r_{min}$ can be shifted by changing the ratio $\gamma = V_{02}/V_{01}$. Case B shows an example of making r_{min} the preferred value for the frequency standard as discussed in Sect. 2.

1.2 DC-Bias Effect

One can improve the pseudopotential-well shape by applying a dc bias to the inner electrode. To calculate Φ_{in}, we use (2) and the boundary conditions with a dc voltage V_{dc} applied to the inner electrode of the ring trap while the other electrodes are grounded. The expression for the electrostatic potential is

$$\Phi_{in}(r,z) = \frac{4V_{dc}}{\pi} \sum_{k=\text{odd}} \frac{1}{k} \frac{I_0^{(2)} K_0\left(\frac{\pi k}{H} r\right) - K_0^{(2)} I_0\left(\frac{\pi k}{H} r\right)}{K_0^{(1)} I_0^{(2)} - K_0^{(2)} I_0^{(1)}} \times \sin\left(\frac{\pi k z}{H}\right). \tag{10}$$

Table 1. Illustrative dimensions and operating parameters for the mercury-ion ring-trap model

Ion:	$^{199}Hg^+$
Atomic weight:	$m = 199$ amu
Hyperfine splitting of $6S_{1/2}$ state (clock transition):	$\nu_a = 40.6$ GHz
Dimensions of ring trap	
Radius of inner cylinder electrode:	$R_1 = 1.0$ mm
Radius of outer cylinder electrode:	$R_2 = 10.0$ mm
Height:	$H = 7.3$ mm
ac and dc voltages:	
Case A ac	$V_{01} = V_{02} = 250$ V
dc	$V_{dc} = 0$ V
Case B ac	$V_{01} = 450$ V
	$V_{02} = 150$ V
dc	$V_{dc} = 0$ V
Case C ac	$V_{01} = V_{02} = 250$ V
dc	$V_{dc} = 30$ V
Drive frequency:	$\Omega = 2\pi\ 1.0$ MHz

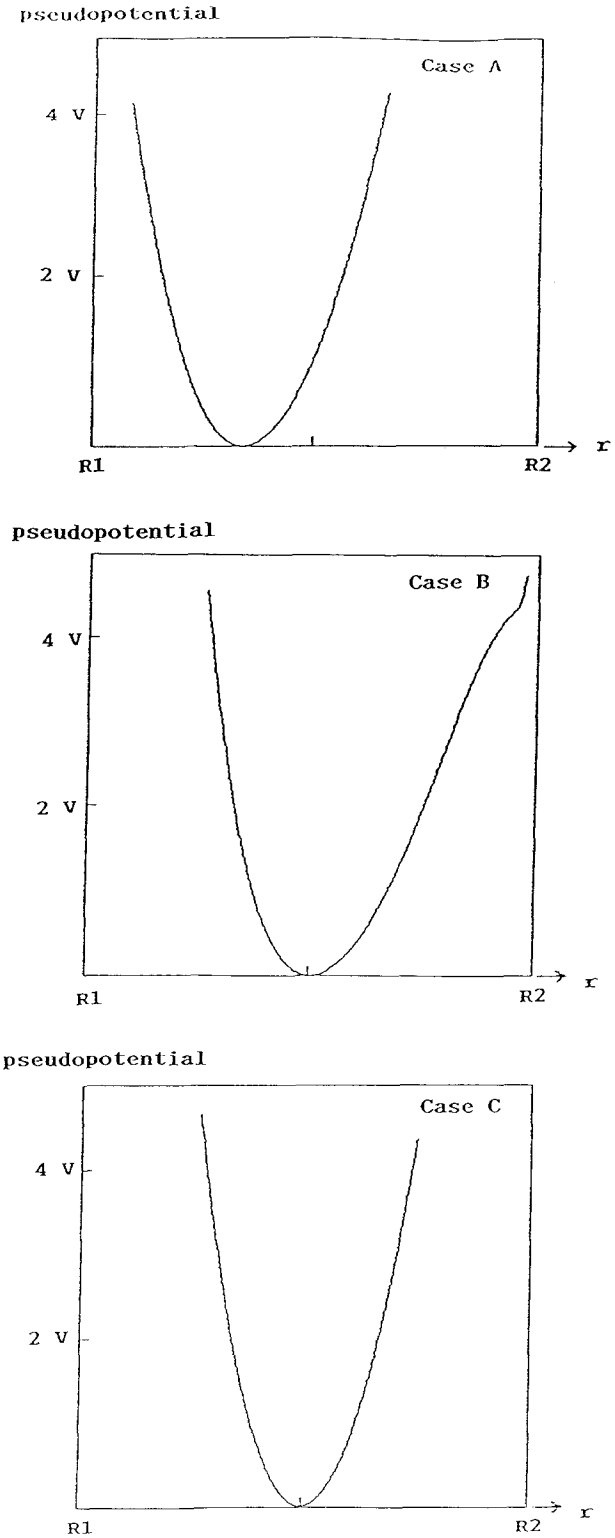

Fig. 3. The dependence of the pseudopotential on r for fixed $z = H/2$. Trapping conditions are listed in Table 1

As shown in Figs. 2 and 3 (Case C) r_{min} can be also shifted by providing a dc bias. Case B is better than Case C because the trapping force along the z-direction is small in Case C (Fig. 2).

1.3 Ion Motion

The obtained pseudopotential determines the trajectory of an ion with the defined e/m ratio in the ring-trap volume. Under certain conditions, the ion moves along the nodes of the trapping field without hitting the electrodes. Vibrational motion of the ion occurs in the plane transverse to the nodal circle [(r, z)-plane], while thermal effects cause the ions to diffuse along the nodal circle at $r = r_{min}$.

Analysis of the ion motion in the ring trap is based on the following equatons:

$$\begin{cases} \ddot{r} - (4eE_r/\Omega^2 m)\cos 2\tau = 0\,, \\ \ddot{z} - (4eE_z/\Omega^2 m)\cos 2\tau = 0\,, \end{cases} \tag{11}$$

where E_r and E_z are derived from (8) and (9). Here the space-charge effect is neglected.

In general, these equations can be solved only numerically, but at first we assume that the ion motion is harmonic in the close vicinity of the node. Numerical calculations following (11) show that this approximation is appropriate. For simplicity we will consider the transverse potential in a 2-dimensional rectangular coordinate system in the plane containing the z-axis (transverse plane). We place the center of the coordinates at the point (r_{min}, z_{min}), whose pseudopotential is minimum (z_{min} is always $H/2$). Thus $r - r_{min}$ is x_r, and $z - z_{min}$ is x_z. The transverse electrostatic potential in the new rectangular coordinate system close to the node can be written as

$$\Phi(x_r, x_z) = (V_{01}/2r_0^2)(\alpha_r x_r^2 - \alpha_z x_z^2)\cos\Omega t\,, \tag{12}$$

where $r_0 = (R_2 - R_1)/2$ and α is a dimensionless coefficient that depends on the electrodes' configuration and γ. The ion motion is obtained solving Mathieu's equations:

$$\ddot{x}_s + 2q_s\cos(2\tau)x_s = 0\,, \qquad s = r, z\,, \tag{13}$$

where $q_s = (2\alpha_s eV_{01})/(\Omega^2 r_0^2 m)$ and $\tau = \Omega t/2$.

The coefficient α_s can be estimated numerically from the pseudopotential. For example in Case B of Table 1, α_r and α_z are 0.59, and q_r and q_z are 0.44. The transverse pseudopotential close to the node is expressed as

$$\Psi(x_r, x_z) = eV_{01}(\alpha_r^2 x_r^2 + \alpha_z^2 x_z^2)/(4m\Omega^2 r_0^4)\,. \tag{14}$$

The secular frequency, $\omega_{r,z}$, can be deduced immediately from the formula

$$\omega_{r,z} = \sqrt{(1/m)\partial^2 U/\partial x_{r,z}^2|_{x_{r,z}=0}}\,, \tag{15}$$

where the pseudopotential energy U is expressed by $U = e\Psi$, and therefore,

$$\omega_{r,z} = q_{r,z}\Omega/(2\sqrt{2})\,. \tag{16}$$

Using the trapping parameters mentioned above,

$$\omega_r = \omega_z = 2\pi\ 157\ \text{kHz}\,. \tag{17}$$

Solutions of these equations appear to be stable when $0 < q < 0.908$ [11]. For larger oscillation amplitudes, the stability conditions are determined not only by q, but also by the values of the initial coordinates [9]. The dependence of the motional stability of the ion on its initial state in the ring trap is obtained by numerical calculations following (11). Figure 4 shows the region of initial positions in which

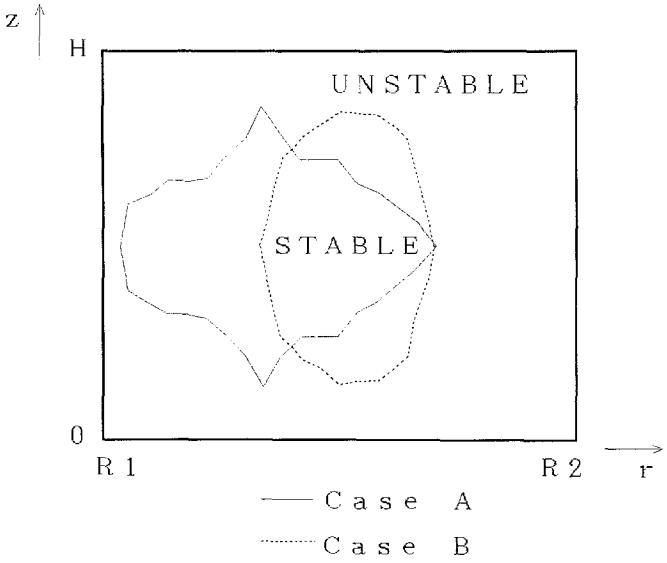

Fig. 4. Diagram of the initial positions of the ion. The contour line separates the stable and unstable regions of ion motion. These contour plots are obtained by numerical calculation. If the ion is created inside the stable region, its vibrations are stable. Otherwise, the vibration amplitude increases until the ion hits one of the electrodes. Trapping conditions are shown in Table 1

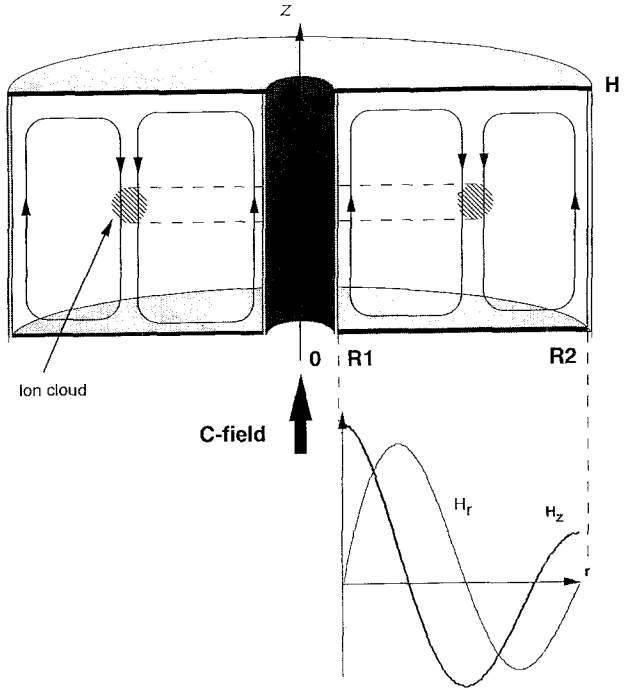

Fig. 5. $TE_{0,2,1}$ microwave field configuration in the ring trap that is appropriate for exciting a magnetic dipole transition between the hyperfine levels of the $^{199}Hg^+$ ground state

the ion motion is stable at $0 < \tau < 1000$. The rf-field phase and initial velocity of the ion are taken to be zero.

2 The Microwave Cavity Mode

The trapping electrodes form a microwave cavity. It is necessary to choose a geometry of the ring-trap cavity and a microwave configuration that are advantageous for application to a frequency standard. A frequency standard is obtained by stabilizing a frequency of a crystal oscillator on the $M = 0 \rightarrow 0$ transition (called the clock transition), as it is independent of magnetic field to first order. Applying a constant magnetic field (called the C-field) separates the clock transition from other transitions.

The microwave mode in the ring trap cavity must satisfy the following two requirements:

(i) The C-field is parallel to the magnetic component of the microwave mode (probe mode) throughout the area in which the ions are trapped;

(ii) Both the microwave field and the C-field are uniform throughout the space in which the trapped ions are localized.

The combination of Helmholtz coils coaxial with the ring trap and the $TE_{0,2,1}$ microwave mode is considered to be the most satisfactory since it is easy to localize ions in the space where the magnetic microwave vector is parallel to the C-field, and there is no first-order Doppler effect for ion motion along the nodal circle in the presence of a microwave field uniform in θ.

The axial, H_z, and radial, H_r, components (Fig. 5) of the microwave probing field for the $TE_{0,2,1}$ mode are expressed as [11, 12]

$$H_z(r,z,t) = H_0 P_0(r)\sin(\pi z/H)\cos(2\pi\nu t)\,,$$

$$H_r(r,z,t) = H_1 P_1(r)\cos(\pi z/H)\cos(2\pi\nu t)\,,$$

$$P_m(r) = J_m(k_c r) + \lambda N_m(k_c r)\,,$$

$$H_1 = -(2\pi\nu/ck_c)H_0\,. \tag{18}$$

Here, J_m and N_m are Bessel functions of mth order and ν is the microwave frequency. Assuming perfectly conducting walls the constants λ and k_c are obtained from the radial boundary conditions:

$$P_1(R_1) = P_1(R_2) = 0\,. \tag{19}$$

There is one solution of r_c:

$$P_1(r_c) = 0\,, \qquad R_1 < r_c < R_2\,. \tag{20}$$

The resonance frequency is expressed as

$$\nu_0 = c\sqrt{(k_c/2\pi)^2 + (1/2H)^2}\,, \tag{21}$$

whre c is the velocity of light.

Under the conditions listed in Table 1, the constants take on the values

$$\lambda = 0.32\,,$$

$$k_c = 0.731/\text{mm}\,,$$

$$r_c = 5.66\ \text{mm}\,,$$

$$\nu_0 = 40.6\ \text{GHz}\,,$$

$$H_1/H_0 = -1.16\,. \tag{22}$$

An ion-trapping system of the size indicated in Table 1 is appropriate for a frequency standard using $^{199}Hg^+$, as ν_0 coincides with the clock transition frequency. Since the

magnetic microwave field is parallel to the C-field at $r = r_c$, the ions should be localized near there.

To obtain a stable $TE_{0,2,1}$ mode, all other modes must be suppressed. As the coaxial cylinders and the two lids are electrically isolated, all modes other than type $TE_{0,n,s}$ are suppressed [13]. The geometry should be such that any other $TE_{0,n,s}$ mode frequency is far from ν_0. With the values shown in Table 1, the cut-off frequencies are higher than ν_0 for $n > 3$. The resonance frequencies of the $TE_{0,1,1}$ and $TE_{0,1,2}$ modes are 27.0 GHz and 44.7 GHz, respectively. Thus, the $TE_{0,2,1}$ mode should oscillate without disturbance.

3 First-Order Doppler Effect

The first-order Doppler effect results from the phase variation of the probed microwave caused by the ion vibration. We calculate the microwave spectrum of the ions using the correlation-function formalism. The first-order Doppler effect in the ring trap should be considered only for vibrations in the r- and z-directions, since the phase distribution is uniform in the θ direction for the $TE_{0,2,1}$ mode. The spectrum of an ion in this case is expressed by

$$I(\omega, \omega_0) = \int_{-\infty}^{\infty} G(t_c)\exp(-i\omega_a t_c)dt_c\,, \tag{23}$$

where $\omega_a = 2\pi\nu_a$ and ν_a is the clock transition frequency. The correlation function $G(t_c)$ is defined as

$$G(t_c) = \lim_{T\to\infty} (1/2T) \int_{-T}^{T} H_{za}(t)H_{za}(t + t_c)dt\,, \tag{24}$$

where $H_{za}(t) = H_z(r, z, t)$ and (r, z) is the position of the ion in the transverse plane.

For the calculation, we consider the ion motion to be a small vibration expressed as

$$r = r_{min} + r_0\cos(\omega_r t)\,, \tag{25}$$

$$z = z_{min} + z_0\cos(\omega_z t)\,, \tag{26}$$

where r_0 and z_0 are the amplitudes of vibrations in the r- and z-directions, which are assumed to be much smaller than the scale of the field gradient. The power spectrum consists of a Doppler-free carrier ($\omega = \omega_0$) and sidebands, expressed as

$$I(\omega, \omega_a) = \sum_{m,n} B_{m,n}\delta(\omega - \omega_a - m\omega_r - n\omega_z)\,, \tag{27}$$

$B_{0,0}$ denotes the carrier intensity, and the remaining $B_{m,n}$ denote the sideband intensities. When the first-order Doppler effect becomes significant, the absorbed power is distributed mainly in the sidebands and the carrier S/N ratio decreases.

To calculate the intensities of the carrier and sidebands we expand $P_0(r)$ and $\cos(\pi z/H)$ as

$$\begin{aligned} P_0(r) = {} & P_0(r_{min}) - P_1(r_{min})k_c r_0\cos(\omega_r t) \\ & + (1/2)(P_1(r_{min})/k_c r_{min} \\ & - P_0(r_{min}))(k_c r_0)^2\cos^2(\omega_r t)\,, \end{aligned} \tag{28}$$

$$\cos(\pi z/H) = \sum_{k=0}^{\infty} J_k(\pi z_0/H)\cos(k\omega_z t)\,. \tag{29}$$

Table 2. Power-distribution spectrum for ring trap and linear trap

Ring trap[a]		Linear trap[b]	
$B_{0,0}$ (carrier)	90.4%	$B'_{0,0}$ (carrier)	26%
$B_{2,0}$	0.8%	$B'_{2,0}$	25%
$B_{-2,0}$	0.8%	$B'_{-2,0}$	25%
$B_{0,1}$	4.0%	$B'_{4,0}$	5%
$B_{0,-1}$	4.0%	$B'_{-4,0}$	5%
		$B'_{0,1}$	2%
		$B'_{0,-1}$	2%

[a] 2×10^7 ions are trapped with the condition in Table 1 (Case B). $B_{m,n}$ are coefficients in (27)
[b] 2×10^7 ions are trapped with the condition in the Appendix. $B'_{m,n}$ are coefficients in (A3)

Here, we consider the condition

$$r_{min} = r_c\,, \tag{30}$$

i.e. the radial position of the minimum in the pseudopotential (Figs. 2, 3) coincides with that of the vanishing radial microwave-magnetic field (20), as it was shown to be a desirable condition for the frequency standard in the previous section. Since $P_1(r_c)$ is zero, (28) can be rewritten as

$$P_0(r) = P_0(r_c)[1 - (1/2)(k_c r_0)^2\cos^2(\omega_r t)]\,. \tag{31}$$

Assuming 2×10^7 ions are trapped under the conditions in Table 1 (Case B), the radius of the ion cloud is 0.93 mm, and the transverse vibrational frequencies are $\omega_r = 157$ KHz $= \omega_z$. The linear trap model examined in the appendix shows a power distribution in the carrier of $B'_{0,0} \approx 26\%$, as compared to the ring-trap carrier power of $B_{0,0} \approx 90\%$ (see Table 2). Since the ring trap concentrates more power in the carrier, it provides a larger S/N ratio compared to the linear trap.

4 Second-Order Doppler Effect

On the basis of the analysis of the ring-trapping system, we conclude that its trapping conditions are similar to those of the rf/dc hybrid linear trapping system because both the rf/dc hybrid linear trap and the ring trap possess a line (or circle) of nodes instead of a single-point node as in the ordinary 3-dimensional Paul trap, and the pseudopotential inside the ring trap may be considered as harmonic in the vicinity of nodes, as our numerical calculations show (Figs. 2, 3).

Taking into account these considerations, the formula for the second-order Doppler shift caused by the trap field (vibration in r- and z-directions) given in [4] is

$$\left(\frac{\Delta\nu}{\nu}\right) = \left(\frac{e^2}{8\pi\varepsilon_0 mc^2}\right)\left(\frac{N}{L}\right), \tag{33}$$

where N is the number of trapped ions, L is the length of the ion cloud, and ε_0 is the permittivity of free space. Analysis of this formula shows that the linear trap has a larger ion-storage capacity for a given second-order Doppler effect than the 3-dimensional Paul trap. To use this formula for ring-trap applicatons one should replace

L with $2\pi r_{\min}$. Using the parameters shown in Table 1, the second-order Doppler shift is expressed as

$$(\Delta\nu/\nu) = 1.0 \times 10^{-19} N \,. \tag{34}$$

The second-order-Doppler shift due to the thermal motion (diffusion along the nodal circle) at room temperature is

$$(\Delta\nu/\nu) = 2.2 \times 10^{-13} \,, \tag{35}$$

as shown in [3, 5]. It is reasonable to associate the thermal motion with the room temperature alone, because the rf heating in the linear trap and ring trap is much less effective than that in the Paul trap [14].

5 Conclusion

The ring-trap model presented has large storage capacity and reduced susceptibility to the second-order Doppler effect. By introducing ac voltage signals to the vertical electrodes a pseudopotential distribution was derived, which was then optimized for applicatons involving frequency standards. The electrodes of the ring trap form a microwave cavity. The microwave phase is uniform with respect to θ. When the condition is optimized for the frequency standard, the absorbed power is concentrated mostly in the carrier. Both the linear trap and the ring trap show a reduced rf-heating effect, compared to the Paul trap, but the ring trap optimized for the frequency standard presented here has a smaller first-order Doppler effect contribution, thus allowing significantly more power to be concentrated at the clock transition frequency than in the linear-trap case.

Acknowledgements. This work was supported by the International Cooperation Project "High Resolution Laser Spectroscopic Techniques", founded by the Science and Technology Agency (S.T.A.) in Japan. We greatly appreciate the encouragement of Dr. Shinji Urabe (K.A.R.C.), Dr. Koji Nakagiri (K.A.R.C.), and Dr. Risao Hayashi (Kagoshima Univ., Japan) throughout this project.

We thank Dr. Yuri Domnin (VNIIFTRI) for the initial discussion of the paper, Mr. Vyacheslav Baryshev (VNIIFTRI) for valuable discussion and Dr. Wayne M. Itano (N.I.S.T., USA) for his important comment on our manuscript.

Appendix

With the linear-trap model, a traveling microwave is used as the probe. Here, we consider the 2-dimensional (X, Z) model, in which X is the direction of the traveling microwave and Z is the direction parallel to the linear electrodes. The X-direction is perpendicular to the Z-direction. We assume that the ion motion is expressed as

$$X = d + X_a \cos\omega_X t \,,$$
$$Z = Z_a \cos\omega_Z t \,, \tag{A1}$$

where X_a, ω_X are the secular vibration amplitude and frequency of the ion along the X-axis, Z_a, ω_Z are the secular vibration amplitude and frequency of the ion along the X-axis, and d is the distance between the trap center and the microwave horn ($X_a \ll d$).

The traveling wave from the microwave horn is expressed as

$$H_Z = H_{Z0} \cos(\omega t - K_0 R) \sin(K_0 b Z/2R)/Z \,, \tag{A2}$$

where $R = (X^2 + Z^2)^{1/2}$ and b is the microwave horn length in the Z-direction. We assume $N = 2 \times 10^7$ trapped ions with the following conditions:

$$d = 175 \text{ mm} \,, \qquad K_0 = 0.85/\text{mm} \,,$$
$$b = 30 \text{ mm} \,, \qquad Z_a = 35\text{mm} \,,$$
$$\omega_X = 157 \text{ kHz} \,, \qquad \omega_Z = \text{arbitrary} \,.$$

The value of ω_X is assumed to be the same as ω_r and ω_z of the ring trap. Thus X_a is 0.65 mm. The other parameters are close to those used in the experiments of Prestage et al. [3–5]. The power distribution spectrum is symmetric around the carrier frequency, and $\omega = \omega_a$ and can be written in a form similar to (27) as

$$I(\omega, \omega_a) = \sum_{m,n} B'_{m,n} \delta(\omega - \omega_a - m\omega_Z - n\omega_X) \,. \tag{A3}$$

Values of $B'_{m,n}$ are shown in Table 2.

References

1. L.S. Cutler, R.P. Giffard, P.J. Wheeler, G.M.R. Winkler: Initial operational experience with a mercury ion storage frequency standard, in *Proc. 41st Ann. Symp. Freq. Control* (IEEE, New York 1987) Cat. No. 87CH2427-3, p. 12
2. R. Blatt, H. Schnatz, G. Werth: Z. Phys. A **312**, 143 (1983)
3. J.D. Prestage, R.L. Tjoelker, G.J. Dick, L. Maleki: J. Mod. Opt. **39** (2), 221 (1992)
4. J.D. Prestage, G.J. Dick, L. Maleki: J. Appl. Phys. **66** (3), 1013 (1989)
5. J.D. Prestage, G.J. Dick, L. Maleki: IEEE Trans. IM-**40** (2), 132 (1991)
6. L.S. Cutler, R.P. Giffard, M.D. McGuire: Appl. Phys. B **36**, 137 (1985)
7. D.A. Church: J. Appl. Phys. **40**, 3127 (1969)
8. I. Waki, S. Kassner, G. Birk, H. Walther: Phys. Rev. Lett. **68**, 2007 (1992)
9. H.S. Lakkaraju, H.A. Schuessler: J. Appl. Phys. **53**, 3967 (1982)
10. H.G. Dehmelt: Adv. At. Mol. Phys. **3**, 53 (1967)
11. W. Paul, M. Raether: Z. Phys. **140**, 262 (1955)
12. M. Benilan, C. Audoin: Int. J. Mass Spectrom. Ion Phys. **11**, 421 (1973)
13. S. Ramo, J.D. Whinnery, T. Van Duzer: *Fields and Waves in Communication Electronics* (Toppan, Tokyo 1965) pp. 446, 550
14. M. Tachikawa, M. Kajita, T. Shimizu: IEEE Trans. IM-**42** (2), 281 (1993)